Observation of surface dispersive shock waves in a self-defocusing medium

Jing Wang,[1,2] Juntao Li,[2] Daquan Lu,[1] Qi Guo,[1] and Wei Hu[1,*]

[1]*Guangdong Provincial Key Laboratory of Nanophotonic Functional Materials and Devices, South China Normal University, Guangzhou 510006, People's Republic of China*

[2]*State Key Laboratory of Optoelectronic Materials and Technologies, School of Physics and Engineering, Sun Yat-Sen University, Guangzhou 510275, People's Republic of China*

(Received 17 February 2015; published 16 June 2015)

We have theoretically and experimentally investigated surface dispersive shock waves (SDSWs) at the interface between a self-defocusing medium and a linear medium. We demonstrate that SDSWs can form when the linear refractive index of the self-defocusing medium is much greater than that of the linear medium, and the initial nonlinearity far outweighs diffraction. SDSWs have been observed at the interface between air and a weakly absorbing liquid when the power of the input beam far exceeds that needed to trap a surface dark soliton. We also observed the formation of SDSWs when an input beam was projected away from the interface, and observed these patterns at the curved surface.

DOI: 10.1103/PhysRevA.91.063819 PACS number(s): 42.65.Tg, 42.65.Jx, 47.40.Nm, 52.35.Tc

I. INTRODUCTION

Dispersive shock waves (DSWs), also known as undular bores or collisionless shock waves, arise from the breaking and mode dispersion of a nonlinear wave. They represent a fundamental type of fluid behavior that has an oscillatory front, appearing near wave-breaking points and expanding afterwards, and necessarily exist in a dispersive fluid with an effective pressure and an intensity or density background that can support undamped waves. Although the study of DSWs started long ago in hydrodynamics [1,2] and theoretical characterizations of such structures have improved steadily [3–5], the field has suffered from a lack of reproducible laboratory experiments. In 1970, Taylor *et al.* were first to observe DSWs in a strongly rarified plasma in a laboratory [6]. Since then, experimental observations of DSWs have been made in many physical systems, such as Fermi gas [7], Bose-Einstein condensates [8–10], and electron beams [11].

Under certain regimes, the behavior of light mimics the dynamics of a fluid [12]. Therefore, an all-optical experimental platform can be proposed for studying the dynamics and observing the formation of DSWs. In nonlinear optics, DSWs were initially studied in optical fibers in the temporal domain [13,14]. Recently, DSWs with a laser beam as an initial input have been the subject of intense study in many optical systems, including photorefractive media [15–17], thermal media [18–24], nematic liquid crystals [25], nonlinear arrays [26], quadratic media [27], disordered media [28], and nonlinear junctions [29]. Here, diffractions result in spatial dispersion that regularizes the shock front through the onset of fast oscillations in an expanding region after the wave-breaking points.

In contrast, surface spatial solitons also have been studied extensively over the last few years [30–33]. Surfaces or boundaries have been found to play an important role in the propagation and stability of nonlocal solitons [31,34,35]. Recently, we investigated the existence and stability of surface dark solitons (SDSs), both theoretically and experimentally [36].

In this research, we undertake further theoretical and experimental investigations of the nonstationary propagation of the SDS at the interface between a nonlocal self-defocusing medium and a linear medium, where the linear refractive index of the self-defocusing medium is much greater than that of the linear medium. Surface dispersive shock waves (SDSWs) have been found to survive in a regime where the initial nonlinearity far outweighs diffraction (i.e., a regime where the background intensity of the input beam far exceeds that needed to trap a fundamental SDS). In this regime, the input beam is attracted towards the interface until it converges to a reflecting point, also called dark focus point or wave-breaking point. After that point, the beam is repelled against the interface and SDSW, composed of one-dimensional black and gray soliton [37] trains, emerges gradually with constant velocity and darkness. These optical SDSWs may find their counterparts in a classical fluid or other fluidlike medium.

II. THEORETICAL MODEL

The light beam dynamics considered here is modeled accurately by the (1+1)-dimensional dimensionless Schrödinger equations

(i) in nonlocal self-defocusing medium, i.e., $x \leqslant 0$,

$$i\frac{\partial u}{\partial z} + \frac{1}{2}\frac{\partial^2 u}{\partial x^2} + \Delta n u = 0, \tag{1}$$

$$\Delta n - \sigma^2 \frac{\partial^2 \Delta n}{\partial x^2} = -|u|^2, \tag{2}$$

(ii) in linear medium, i.e., $x > 0$,

$$i\frac{\partial u}{\partial z} + \frac{1}{2}\frac{\partial^2 u}{\partial x^2} - n_d u = 0. \tag{3}$$

Here, $u(x,z)$ is the complex amplitude envelope of the light beam, where x and z stand for the transverse and longitudinal coordinates. Δn denotes the nonlinear index change in the nonlocal self-defocusing medium. σ represents the degree of nonlocality of the nonlinear response. $n_d > 0$ describes the difference in the linear refractive index between the nonlocal self-defocusing medium and the linear medium.

In addition, we address a TE polarized light beam, where the continuity of the transverse field implies $u(x = +0) =$

*Corresponding author: huwei@scnu.edu.cn

$u(x=-0)$. In our dimensionless system, the value of n_d is much greater than the actual difference in the linear refractive index between the nonlocal self-defocusing medium and the linear medium [33]. When the actual linear refractive index of the nonlocal self-defocusing medium and the linear medium are n_0 and n_L, the dimensionless index difference $n_d = (n_0^2 - n_L^2)k_0^2 w_a^2/2$, where k_0 is the wave number in vacuum and w_a is a characteristic length of beamwidth used for normalization. In most experiments, we have $(k_0 w_a)^2 \gg 1$ for any paraxial beams. Therefore, $n_d \gg 1$ is easily satisfied even for a relative small difference between n_0 and n_L. Details can be found in Ref. [33]. When $n_d \gg 1$, almost all the light beams will propagate in the higher-index nonlinear medium [31]. Here, we choose $n_d = 500$ in numerical simulations. The asymptotic behaviors of SDSWs when $x \to -\infty$ are similar to those of bulk DSWs [21]. For the theoretical study of SDSWs in this paper, $\partial u/\partial x|_{x\to-\infty} = 0$ are used in numerical simulations for convenience. According to the experimental instance [31], the boundary condition for the nonlinear index change is assumed to be $\partial \Delta n/\partial x|_{x=0} = 0$ and $\Delta n(x \to -\infty) = 0$. For a thermal nonlocal nonlinear medium, this implies that the interface between the nonlinear and linear medium is thermally insulating and the other surface of the nonlinear medium is thermally conducting.

To gain a better understanding of shock behavior, it is instructive to express Eq. (1) in a hydrodynamic form by applying the transformation $u(x,z) = \sqrt{\rho(x,z)}\exp[i\phi(r,z)]$, where $\rho = |u|^2$ plays the role of the density of an optical fluid and ϕ is the corresponding phase. Separating real and imaginary components yields two Euler-like fluid equations

$$\frac{\partial \rho}{\partial z} + \frac{\partial(\rho v)}{\partial x} = 0, \tag{4}$$

$$\frac{\partial v}{\partial z} + v\frac{\partial v}{\partial x} = \frac{\partial \Delta n}{\partial x} + \frac{1}{2}\frac{\partial}{\partial x}\left(\frac{1}{\sqrt{\rho}}\frac{\partial^2\sqrt{\rho}}{\partial x^2}\right). \tag{5}$$

Here the spatial chirp $v = \partial\phi/\partial x$ plays the role of the transverse velocity of an optical fluid. Eq. (4) expresses conservation of power during propagation of a light beam along the z axis, whereas Eq. (5) is a momentum equation describing that optical flow results from nonlinear pressure and diffraction. Diffraction always makes the input beam flow away from the surface, whereas the nonlocal self-defocusing nonlinearity causes the beam to flow towards the regions of low intensity (i.e., the vicinity of the surface). The surface is equivalent to a potential barrier that prevents the beam from flowing into the linear medium. Because of the rejection of the surface, a beam flowing into the surface converges to a dark focus point corresponding to an infinite gradient of the hydrodynamic type around a point of vanishing intensity. Around the focus point, the beam begins to divide. After the focus point, SDSW is progressively manifested. It consists of distinctive one-dimensional black and gray soliton trains and maintains a fixed velocity and darkness flowing away from the surface.

III. NUMERICAL SIMULATIONS

Numerical simulations of SDSWs at the interface between a nonlocal self-defocusing medium and a linear medium are based on Eqs. (1)–(3). Here, the input amplitude envelope $u(x,z=0) = NW(x)$, where $W(x)$ is a fundamental SDS solution of these equations [36] and N^2 describes the intensity of the background. $N^2 = 1$ shows that the initial nonlinear effect balances the diffraction, whereas $N^2 > 1$ shows that the initial nonlinear effect is stronger than the diffraction. The diffraction effect makes the input beam move away from the surface in the x-axis direction, during propagation in the z-axis direction. In addition, it also makes the transverse velocity v of the optical fluid in the x-axis direction greater where the background intensity is greater. The beam then will spread under the diffraction effect. In contrast, nonlocal defocusing nonlinearity makes the beam move towards the surface in the x-axis direction during propagation in the z-axis direction. When the two effects mutually balance, the beam will SDS propagate. When the initial nonlinear effect is much stronger than the diffraction, the beam will propagate in the form of SDSWs.

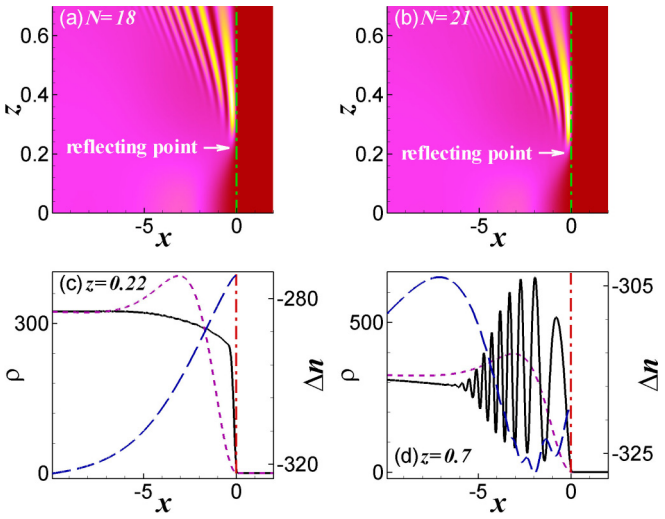

FIG. 1. (Color online) Numerical simulation of SDSWs based on Eqs. (1)–(3) with $\sigma = 2.4$. (a), (b) Propagation of SDSWs for different N. (c), (d) Snapshots of case (a) at a different propagation distance z: nonlinear index change (blue long-dashed curve) and optical fluid density (black solid curve) compared with the input beam (dashed curve). Dashed-dotted lines show the interface.

A group of typical SDSW results is shown in Fig. 1. A smooth input beam [Figs. 1(a) and 1(b)], the profile of which is shown in Figs. 1(c) and 1(d), will move progressively towards the surface in the x-axis direction during propagation in the z-axis direction until it converges to a reflecting point (i.e., wave-breaking point) at a finite distance. At the z-axis position of this reflecting point, the profile of the beam, as shown in Fig. 1(c), becomes very steep in the vicinity of surface, where the gradient of the beam is very large. The convergence of the beam increases the strength of the diffraction effect. Beyond that point, diffraction regularizes the front through the gradual appearance of black and gray soliton trains (i.e., SDSWs) as shown in Fig. 1(d). The angle of the black and gray solitons with the propagation direction (i.e., transverse velocity v) increases as their relative darkness decreases as displayed in Figs. 1(a) and 1(b). In particular, the transverse velocity of the black soliton is zero and it propagates parallel to the surface.

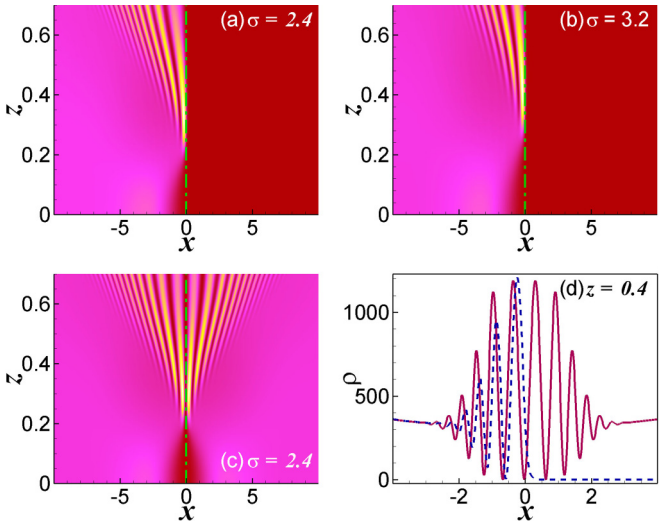

FIG. 2. (Color online) Impact of nonlocality degree on SDSW and relationship between SDSW and bulk DSW with $N = 21$. (a)–(c) Propagation of SDSWs and bulk DSW. (d) Comparison of DSW profiles between (a) and (c) at a certain distance. Dashed-dotted lines show the interface or the symmetry axis of bulk DSW.

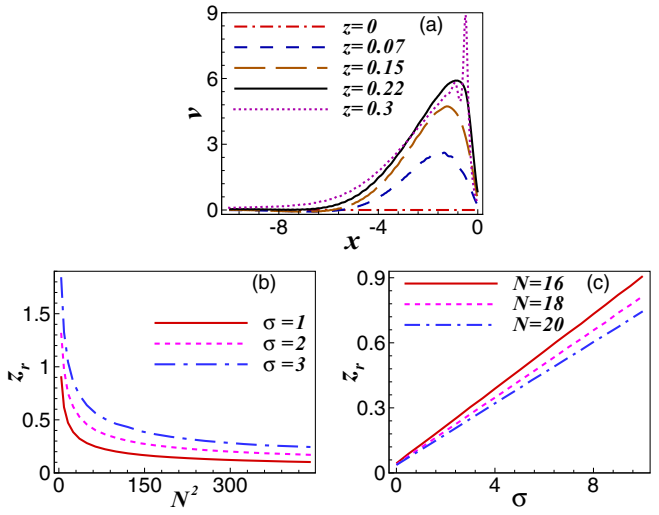

FIG. 3. (Color online) Determination of the reflecting distance and its functional relationship with N^2 and σ. (a) Chirp profile for various z with $N = 18$, and $\sigma = 2.4$. (b) The reflecting distance vs N^2 for different σ. (c) The reflecting distance vs σ for various N.

A comparison of Figs. 1(a) and 1(b) shows that the number of black and gray soliton trains increases for larger N. In particular, the SDSW is composed of half a black soliton and $N' - 1$ gray solitons, where $N' = N$ for integer values of N or the closest integer to it when N is not an integer. From Figs. 1(c) and 1(d), we can also see that the nonlinear index change is very steep at the breaking point and subsequently becomes smooth and fluctuating corresponding to the oscillatory front.

Next we investigate the impact of nonlocality degrees on SDSWs and the relationship between SDSWs and bulk DSWs. A group of typical SDSWs with different nonlocality degrees is shown in Fig. 2(a) and 2(b). A comparison of the SDSWs shows that the number of black and gray soliton trains decreases as the degree of nonlocality degree observed at a certain distance (e.g., at $z = 0.7$) increases. However, the degree of nonlocality does not qualitatively change the number of black and gray soliton trains if we observe them at a great enough distance from where the SDSWs were formed. It merely retards the breaking of the beam and the formation of SDSWs, and broadens the region of black and gray soliton trains. From Fig. 2(d), or by comparing Fig. 2(a) and 2(c), we find that a SDSW in nonlocal self-defocusing media can be regarded as half of a bulk DSW with an antisymmetric amplitude distribution. The relationship has also been found between surface solitons and bulk solitons in nonlocal nonlinear media [33,38].

Further insight into the behavior of SDSWs can be gained by determining the reflecting distance and finding its functional relationships with background intensity N^2 and nonlocality degree σ. The simulated results are shown in Fig. 3. The reflecting point corresponding to $|\partial v/\partial x| \propto \infty$ is found at $x_r = 0$ [Fig. 3(a)]. The reflecting distance z_r decreases monotonously with increasing N^2 as displayed in Fig. 3(b) and increases linearly with increasing σ as revealed in Fig. 3(c). This is because an increase in the background intensity makes the input beam converge more quickly to the surface and then form a reflecting point. In contrast, the nonlocality degree tends to weaken nonlinearity and slows the convergence of the input beam to the surface.

IV. EXPERIMENTAL RESULTS

Experimental observations of SDSWs were performed at the interface between diluted India ink (a solution of carbon in water) and air, where the dilution was made by adding 1 mL India ink to 20 L pure water. The solution was contained in a designed cell of dimensions 16 mm × 16 mm × 15 mm in the x, y, and z (propagation) directions, respectively. Here, the bottom and lateral faces of the cell were made of 1-cm-thick copper for conducting heat and maintaining temperature. The top face of the cell was exposed to air to form a thermal insulating interface. Additionally, the input and output faces of the cell were made of 0.3-mm-thin glasses for propagating SDSWs. It is noteworthy that the solution is a thermally nonlocal self-defocusing medium. The carbon in the solution absorbs the light and subsequently creates a thermal gradient in response to the light intensity. The heat diffuses throughout the sample cell and produces a nonlocal index of refraction by way of the thermo-optic effect. Neglecting the effects of convection, the resulting system can be described by Eqs. (1) and (2) [18].

The experimental setup is shown in Fig. 4. A laser beam with a wavelength of 532 nm and a $1/e^2$ beam width of 1 mm

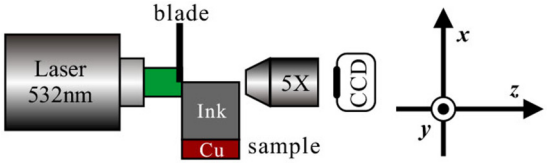

FIG. 4. (Color online) Sketch of the experimental setup.

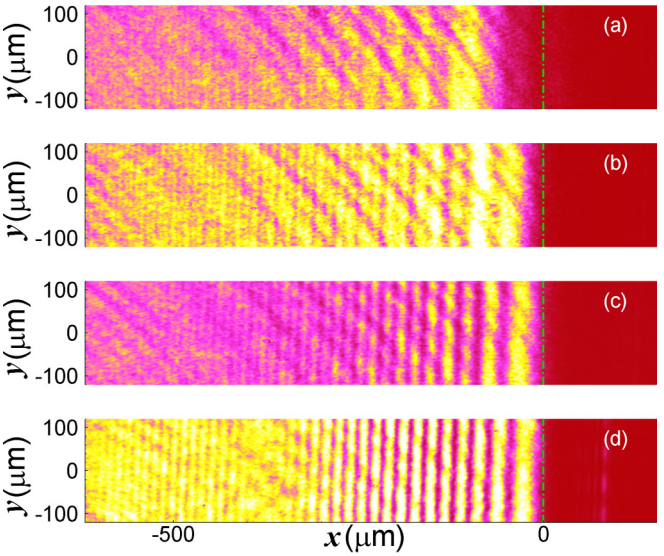

FIG. 5. (Color online) Observations of SDSWs. Intensity distribution of the output beam, collected at the output face of the cell (x-y plane), for different input powers: (a) $P = 2$ mW, (b) $P = 1.68$ W, (c) $P = 2.51$ W, (d) $P = 5.24$ W, which is almost y invariant. Dashed-dotted lines show the interface.

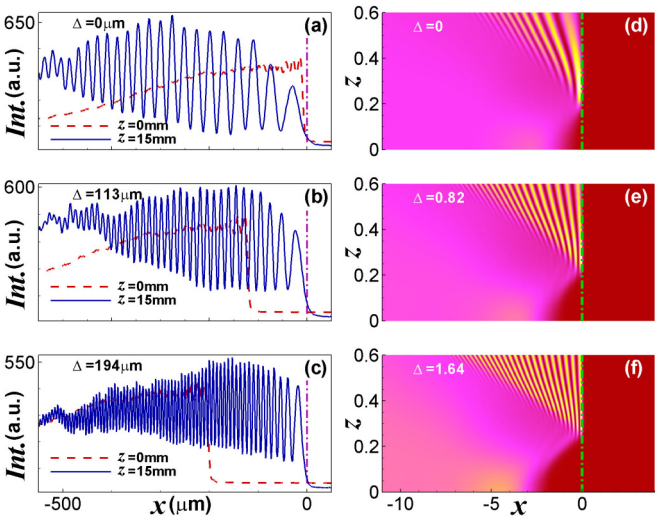

FIG. 6. (Color online) (a)–(c) Experimental observations and (d)–(f) simulation comparison of SDSWs when the input beam is projected Δ away from the air-solution interface in the x-axis direction. (a)–(c) The profiles of the input beams ($z = 0$ mm) and the SDSWs ($z = 15$ mm) are obtained through the average of the intensity distribution (almost y-invariant) at the input and output face of the cell along the y-axis direction. The input power is 5.24 W. (d)–(f) The nonlocality degree $\sigma = 2.4$ and background intensity $N = 21$. Dashed-dotted lines show the interface.

was half blocked by a blade at the input face ($z = 0$ mm) of the cell, and then projected onto the solution parallel to and along the interface between the solution and the air. Then, we observed the intensity distribution at the output face ($z =$ 15 mm) of the cell by imaging the output beams with a charge-coupled device (CCD) camera.

We performed a series of experiments to observe the formation of SDSWs. A group of typical results is shown in Fig. 5. At a low power of 2 mW, the nonlinear effect is very weak. The input beam projected along the interface spreads and its beam edge gradually leaves the interface during the propagation due to diffraction. As shown in Fig. 5(a), the dark stripe becomes very wide at the output face. By increasing the input beam power to 1.68 W, the nonlinear effect is observed to strengthen and balance diffraction. The input beam shrinks towards the surface during propagation. The dark stripe becomes very narrow at the output face and forms a SDS, as shown in Fig. 5(b). When the input power increases further to 2.51 W, the initial nonlinear effect is much stronger than the diffraction. The beam splits into many filaments consisting of black and gray soliton trains and forms a SDSW, as shown in Fig. 5(c). By increasing the input power further to 5.24 W, the beam splits even further, as shown in Fig. 5(d). A comparison of Figs. 5(c) and 5(d) shows that the number of black and gray soliton trains grows with power. It is noteworthy that the distribution of the optical density is almost invariant along y, as expected. This validates the assumption in the model of a y-invariant system. These experimental results are qualitatively consistent with the above numerical results.

We next observed the formation of SDSWs when the input beam is projected away from the air-solution interface in the x-axis direction. The sample cell was moved up and down in the x-axis direction, in order to control the distance Δ between the input beam edge blocked by the blade and the interface, that is the distance of the input beam away from the interface. In our system, the intensity distribution of the optical beams over the propagation lengths involved is almost invariant along y. The intensity distribution of the input beams and the SDSWs recorded at the input ($z = 0$ mm) and output ($z = 15$ mm) face of the cell is averaged along the y-axis direction to convert into the profiles of the input beams and the SDSWs.

A group of typical experiment results is shown in Fig. 6(a)–6(c). Here, we first observed the formation of SDSWs when the input beam is projected along the interface. Figure 6(a) shows the profiles of the SDSW ($z = 15$ mm) and the corresponding input beam ($z = 0$ mm). Then, we observed the formation of SDSWs when the input beam is projected 113 μm away from the interface, as shown in Fig. 6(b). Figure 6(c) shows the formation of SDSWs when the input beam is projected 194 μm away from the interface. We can see that the filamentization number increases with increasing the distance. This is because the velocity of the beam arriving at the interface increases as the distance increases. The collision of the beam with the interface will be stronger and the dispersive shock behavior reflected by the interface will also be more obvious.

Figures 6(d)–6(f) show a group of typical numerical results as comparison. Figure 6(d) shows the formation of SDSWs when the input beam propagates along the interface. Figures 6(e) and 6(f) show the formation of SDSWs when the input beam propagates 0.82 and 1.64 away from the interface. We can see that the filamentization number increases with increasing distance. The numerical simulation agrees qualitatively with the experimental results.

Finally, we observed the formation of SDSWs along curved surfaces. The input beams were projected along the rim of the cell, i.e., the $x = 0$ face. The amount of the solution in a cell

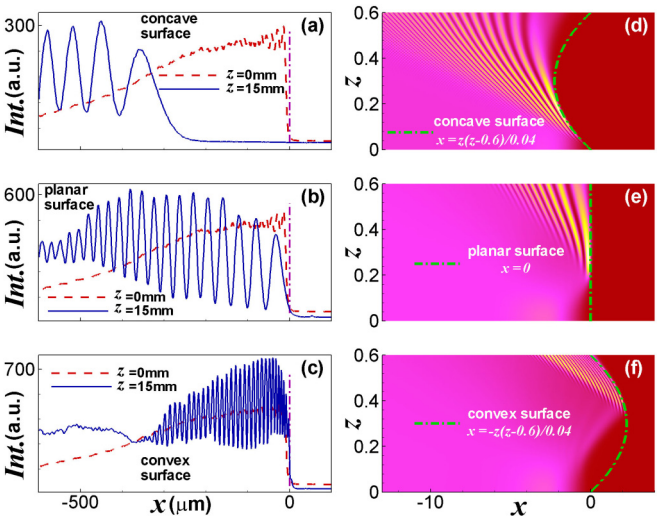

FIG. 7. (Color online) (a)–(c) Experimental observations and (d)–(f) simulation comparison of SDSWs forming along curved surfaces. (a)–(c) The profiles of the input beams ($z = 0$ mm) and the SDSWs ($z = 15$ mm) are obtained through the average of the intensity distribution (almost y invariant) at the input and output face of the cell along the y-axis direction. The input power is 5.24 W. (d)–(f) The nonlocality degree $\sigma = 2.4$ and background intensity $N = 21$. Dashed-dotted lines show the interface.

was adjusted to change the shape of the surface of the solution. The intensity distribution of the input beams and the SDSWs recorded at the input ($z = 0$ mm) and output ($z = 15$ mm) face of the cell is also averaged along the y-axis direction to convert into the profiles of the input beams and the SDSWs.

A group of typical experiment results and simulation comparison is shown in Fig. 7. First, we observed the formation of SDSWs along a concave surface. Figure 7(a) shows the profiles of the SDSW ($z = 15$ mm) and the corresponding input beam ($z = 0$ mm). Figure 7(d) is a simulation comparison in this case. Here the input beam propagates in the z direction along the concave surface $x = z(z - 0.6)/0.04$. Then, we observed the formation of SDSWs along a planar surface. The SDSW result and the corresponding input beam is shown in Fig. 7(b). The corresponding simulation comparison is shown in Fig. 7(e), where the input beam propagates in the z direction along the planar surface $x = 0$. Figure 7(c) shows the result of SDSW formed along a convex surface with the corresponding input beam. The corresponding simulation comparison is shown in Fig. 7(f), where the input beam propagates in the z direction along the convex surface $x = -z(z - 0.6)/0.04$. Compared with SDSWs at the planar surface, SDSWs at the concave surface become thin, whereas SDSWs at the convex surface become thick. This is because the beam will arrive at a concave surface after traveling a shorter distance with a lower velocity, and similarly arrive at a concave surface after traveling a longer distance at a higher velocity. The experimental results agree qualitatively with the numerical simulations.

V. CONCLUSIONS

We can summarize our investigation of surface dispersive shock waves (SDSWs) composed of black and gray soliton trains by considering both theoretical and experimental approaches. Theoretically, we found that SDSWs can form at an interface between a self-defocusing medium and a linear medium, when the linear refractive index of the self-defocusing medium is much greater than that of the linear medium, and the initial nonlinearity far outweighs diffraction. The number of black and gray soliton trains increases as the background intensity increases, and the nonlocality degree does not qualitatively affect this scenario. In fact, a SDSW in a self-defocusing medium can be regarded as half of a bulk dispersive shock wave (DSW).

Experimentally, we observed SDSWs at the interface between air and a weakly absorbing liquid (diluted India ink) when the input power far exceeds that needed to trap a surface dark soliton. We also observed SDSWs when an input beam was projected away from the interface, and observed them at curved surfaces. The experimental results are qualitatively consistent with the numerical results. Such SDSWs integrate the unique features of both surface waves and DSWs in bulk self-defocusing media. These results may motivate further study of DSWs in conjunction with surface waves.

ACKNOWLEDGMENTS

This research was supported by the National Natural Science Foundation of China (Grants No. 11174090 and No. 11174091), the China Postdoctoral Science Foundation (Grant No. 2015M572395), and the Scientific Research Foundation of the Department of Education of Guangdong Province (Grant No. 2013CXZDA012). We thank the referees for their detailed comments that have helped improve this paper substantially.

[1] T. B. Benjamin and M. J. Lighthill, Proc. R. Soc. A **224**, 448 (1954).
[2] D. H. Peregrine, J. Fluid Mech. **25**, 321 (1966).
[3] A. V. Gurevich and A. L. Krylov, Sov. Phys. JETP **65**, 944 (1987).
[4] G. A. El, Chaos **15**, 037103 (2005).
[5] J. Garnier, G. Xu, S. Trillo, and A. Picozzi, Phys. Rev. Lett. **111**, 113902 (2013).
[6] R. J. Taylor, D. R. Baker, and H. Ikezi, Phys. Rev. Lett. **24**, 206 (1970).
[7] J. A. Joseph, J. E. Thomas, M. Kulkarni, and A. G. Abanov, Phys. Rev. Lett. **106**, 150401 (2011).
[8] Z. Dutton, M. Budde, C. Slowe, and L. V. Hau, Science **293**, 663 (2001).
[9] M. A. Hoefer, M. J. Ablowitz, I. Coddington, E. A. Cornell, P. Engels, and V. Schweikhard, Phys. Rev. A **74**, 023623 (2006).
[10] J. J. Chang, P. Engels, and M. A. Hoefer, Phys. Rev. Lett. **101**, 170404 (2008).
[11] Y. C. Mo, R. A. Kishek, D. Feldman, I. Haber, B. Beaudoin, P. G. O'Shea, and J. C. T. Thangaraj, Phys. Rev. Lett. **110**, 084802 (2013).
[12] J. Fatome, C. Finot, G. Millot, A. Armaroli, and S. Trillo, Phys. Rev. X **4**, 021022 (2014).

[13] W. J. Tomlinson, R. H. Stolen, and A. M. Johnson, Opt. Lett. **10**, 457 (1985).
[14] Joshua E. Rothenberg and D. Grischkowsky, Phys. Rev. Lett. **62**, 531 (1989).
[15] W. Wan, S. Jia, and J. Fleischer, Nat. Phys. **3**, 46 (2007).
[16] W. Wan, D. V. Dylov, C. Barsi, and J. W. Fleischer, Opt. Lett. **35**, 2819 (2010).
[17] G. A. El, A. Gammal, E. G. Khamis, R. A. Kraenkel, and A. M. Kamchatnov, Phys. Rev. A **76**, 053813 (2007)
[18] C. Barsi, W. Wan, C. Sun, and J. W. Fleischer, Opt. Lett. **32**, 2930 (2007).
[19] N. Ghofraniha, C. Conti, G. Ruocco, and S. Trillo, Phys. Rev. Lett. **99**, 043903 (2007).
[20] C. Sun, C. Barsi, and J. W. Fleischer, Opt. Express **16**, 20676 (2008).
[21] C. Conti, A. Fratalocchi, M. Peccianti, G. Ruocco, and S. Trillo, Phys. Rev. Lett. **102**, 083902 (2009).
[22] A. Armaroli and S. Trillo, and A. Fratalocchi, Phys. Rev. A **80**, 053803 (2009).
[23] S. Malaguti, A. Corli, and S. Trillo, Opt. Lett. **35**, 4217 (2010).
[24] S. Gentilini, N. Ghofraniha, E. DelRe, and C. Conti, Phys. Rev. A **87**, 053811 (2013).
[25] G. Assanto, T. R. Marchant, and N. F. Smyth, Phys. Rev. A **78**, 063808 (2008).
[26] S. Jia, W. Wan, and J. W. Fleischer, Phys. Rev. Lett. **99**, 223901 (2007).
[27] M. Conforti, F. Baronio, and S. Trillo, Opt. Lett. **38**, 1648 (2013).
[28] V. Folli and C. Conti, New J. Phys. **15**, 085026 (2013).
[29] W. Wan, S. Muenzel, and J. W. Fleischer, Phys. Rev. Lett. **104**, 073903 (2010).
[30] S. R. Skinner and D. R. Andersen, J. Opt. Soc. Am. B **8**, 759 (1991).
[31] B. Alfassi, C. Rotschild, O. Manela, M. Segev, and D. N. Christodoulides, Phys. Rev. Lett. **98**, 213901 (2007).
[32] F. Ye, Y. V. Kartashov, and L. Torner, Phys. Rev. A **77**, 033829 (2008).
[33] Z. Yang, X. Ma, D. Lu, Y. Zheng, X. Gao, and W. Hu, Opt. Express **19**, 4890 (2011).
[34] J. Wang, Y. Li, Q. Guo, and W. Hu, Opt. Lett. **39**, 405 (2014).
[35] J. Wang, Z. Ma, Y. Li, D. Lu, Q. Guo, and W. Hu, Phys. Rev. A **91**, 033801 (2015).
[36] X. Gao, J. Wang, L. Zhou, Z. Yang, X. Ma, D. Lu, Q. Guo, and W. Hu, Opt. Lett. **39**, 3760 (2014).
[37] Y. S. Kivshar and G. P. Agrawal, *Optical Solitons: From Fibers to Photonic Crystals*, sec. 1.4.3 (Academic Press, San Diego, 2003).
[38] X. Ma, Z. Yang, D. Lu, Q. Guo, and W. Hu, Phys. Rev. A **83**, 033829 (2011).